DESIGN AND CONSTRUCTION OF THE LOW-NOISE WIND TUNNEL IN AACHEN

S. Hille*, E. Stumpf*
* RWTH Aachen University, Institute of Aerospace Systems, Wüllnerstr. 7, 52062 Aachen, Germany

Abstract

The newly designed aeroacoustic wind tunnel in Aachen (*German:* **Sch**allarmer **W**indkanal **A**ache**n**, SCHWAN) is an open-circuit, open-jet tunnel with a design velocity of $50\,\mathrm{m/s}$ and a test section of $1.0\,\mathrm{m}$ by $0.8\,\mathrm{m}$ by $2.6\,\mathrm{m}$ (w×h×l). The facility, which at the time of this publication is under construction, is to be integrated into an existing structure by a large extend. The unique conditions yield to some uncommon aspects within the design process, which is documented in this paper. The focus lies on decisions made concerning the general concept, the sizing and positioning of the drive and the design of an expanding corner.

Keywords

aeroacoustics; noise; wind tunnel design; sizing; expanding corner

NOMENCLATURE

Symbols

b	gap width	m
c	speed of sound	$\frac{\mathrm{m}}{\mathrm{s}}$
D	acoustic dampening	dB
e	expansion ratio	-
f	frequency	Hz
L_i	sound pressure level (immission)	dB
L_W	sound pressure level (emmission)	dB
M	Mach number	-
O	circumference of lining	m
S	free cross section area	m^2
u_∞	approach/inflow velocity	$\frac{\mathrm{m}}{\mathrm{s}}$
$\vec{v}$	local flow velocity	$\frac{\mathrm{m}}{\mathrm{s}}$
v	local flow velocity in y-direction	$\frac{\mathrm{m}}{\mathrm{s}}$
X_n, Y_n	dimension, normalized by inflow width	m
X_N, Y_N	dimension, normalized by outflow width	m
α	absorption coefficient	-

Abbreviations

ILR	Institute of Aerospace Systems	
SPL	sound pressure level	dB

1. INTRODUCTION

Aeroacoustics is playing an increasingly important role in the aviation research landscape. Especially in the field of air taxis and unmanned aviation, the need for research on this topic is increasing. With the current megatrends of 'Urban Air Mobility' and 'Urban Air Freight' using air taxis and drones, the enormous economic potential goes hand in hand with the challenge of creating acceptance of these new transport systems among citizens and consumers. The requirement for a design that is as quiet as possible with robust flight characteristics has a particularly high priority.
In the course of these current developments, the Institute of Aerospace Systems (ILR) at RWTH Aachen University is expanding its research infrastructure by an aeroacoustic wind tunnel, the measuring section of which will be integrated into an existing anechoic chamber. The paper at hand introduces the general concept of this new wind tunnel and discusses the design decisions made.

2. THE WIND TUNNEL CONCEPT

After a classification of the new wind tunnels design missions, the existing infrastructure of the anechoic chamber as well as the surrounding construction will be introduced in this section. From these given factors, the overall wind tunnel concept will be deduced, taking into account the top-level design requirements of an aeroacoustic facility.

2.1. General Purpose

The overall purpose of the wind tunnel as a research facility is to enable a detailed investigation of aeroa-

doi:10.25967/530124

coustic phenomena of several classes of test objects. The successive application of microphone arrays, flow visualization and quantitative measurement enables the detailed psycho-acoustic analysis of noise sources and the deduction of constructive measures to reduce disturbing emissions. Considering the aforementioned scenarios, a special interest will lie on the noise sources of air taxies (general aviation) and drones (model airplanes). In addition, related objects such as wind turbines or bluff bodies like passenger cars or buildings might be investigated as well. As an orientation for wind tunnel sizing, the flight speed over Reynolds number of several objects is depicted in figure 1. It can be seen that similar flow conditions for model airplanes and wind turbines can be easily reached with maximum Reynolds numbers up to 1 Mio. Due to their size, general aviation airplanes require a higher value by factor 10, promoting the investigation on half-models or only certain components.

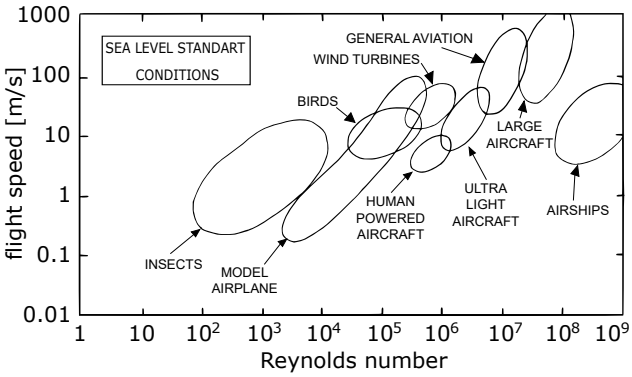

FIG 1. Flight Reynolds number spectrum, cf. [1]

2.2. Geometrical Conditions

The anechoic chamber at the ILR is lined with perforated panel absorbers [2] of 300 mm thickness. In figure 2 the floor plan of the Acoustic Lab with its most relevant dimensions is shown. The anechoic chamber is placed on an own decoupled foundation within a large room of the institute's building. It can be accessed through an acoustically sealed door and has a walkable floor grid that is removable if any interference with the measurement is to be expected. It is obvious, that in this case the integration of an acoustic wind tunnel is highly dependent on the surrounding structure due to the size of the immobile chamber itself as well as its proximity to the surrounding walls, especially since the alteration of the building's facade is prohibited.

2.3. General Design

The general aerodynamic objective of a wind tunnel is to achieve the highest possible flow velocity, with good flow uniformity, both spatial and temporal, in the largest test section size possible [3]. Operation costs favor a closed loop wind tunnel due to recovery of flow energy, however in this case, several criteria indi-

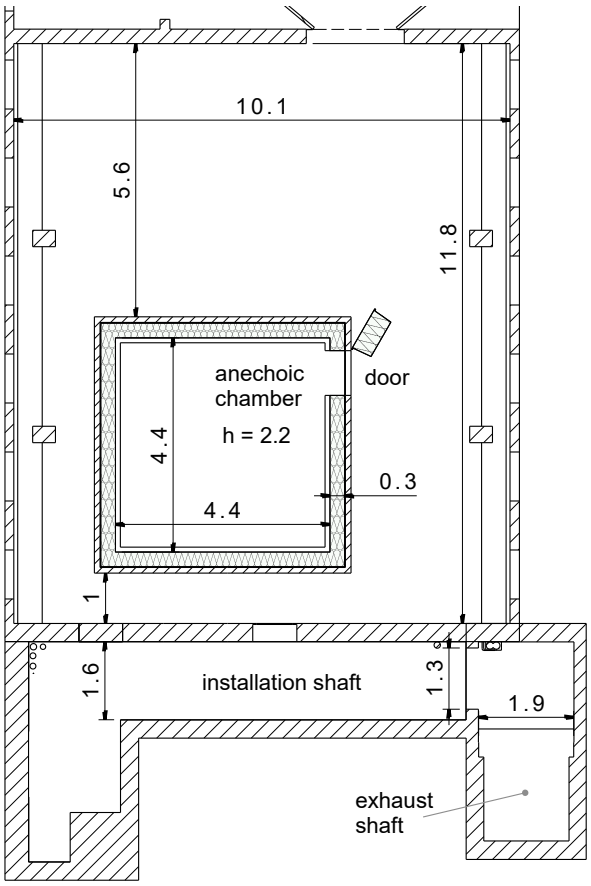

FIG 2. The Acoustic Lab at ILR before wind tunnel integration; dimensions in m

cate against it. The only aerodynamically convenient positioning of settling chamber and contraction is on the open space in front of the chamber, resulting in a counter-clockwise closed loop. On the one hand, for a closed loop to fit within the given structure it would be very restricted in size, only allowing either a small width of the cross section or a small contraction ratio of the nozzle, resulting in lesser flow quality. On the other hand, the wind tunnel drive would have to be positioned in proximity to the test section, resulting in an adversely solution from an acoustic point of view as well. Beyond that, accessibility of the anechoic chamber would be compromised by a large extend.

Therefore it was decided to design an open loop wind tunnel, the downstream duct of which would continue horizontally in an installation shaft and then vertically in a disused exhaust shaft of firmer test beds, as depicted in figure 3. For acoustic measurements, the test section is to remain open so that the anechoic chamber forms the wind tunnel plenum. Due to building statics, the first diffuser, and with it all upstream components, had to be placed asymmetrically to the anechoic chamber, which influences the maximum open jet section achievable without major disturbing secondary flows within the plenum, as will be discussed in subsection 3.1.

The downside of this duct configuration compared to a classic, straight open-circuit tunnel is that in this case four corners have to be incorporated. Nevertheless, it

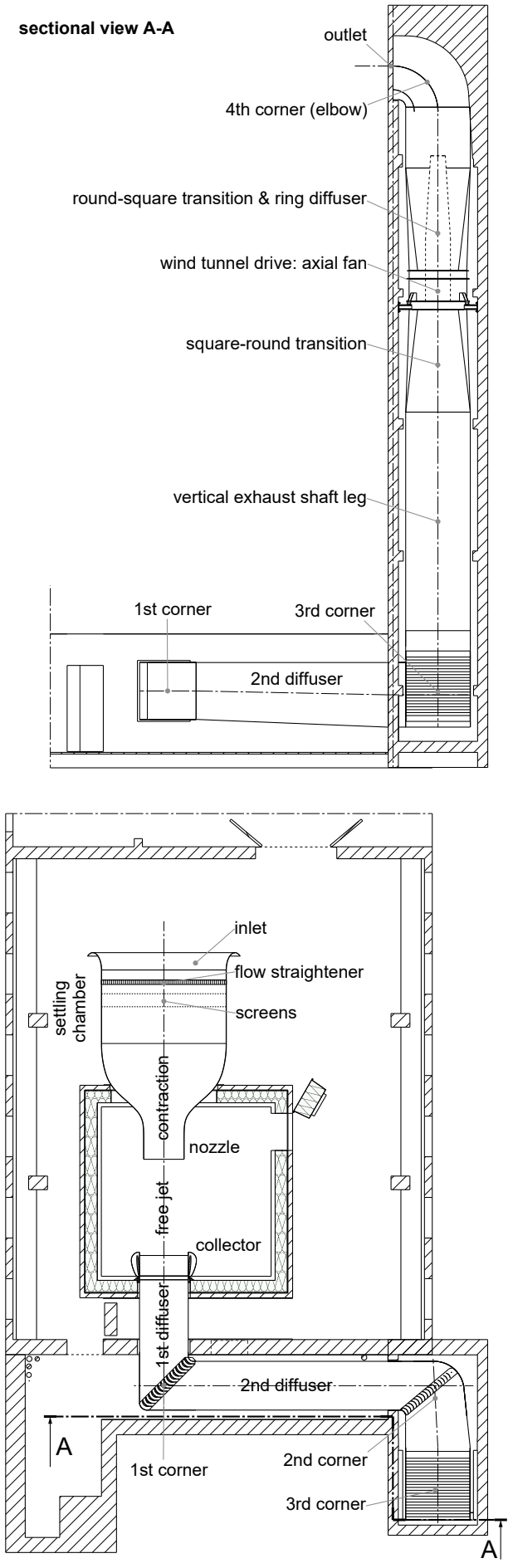

FIG 3. Layout and components of the acoustic wind tunnel of the ILR

also yields the potential for high flow quality within the test section, since the air is accelerated from very low speed, as well as for sufficient acoustical treatment of the ductwork upstream of the drive. The optimal position of which was determined to be as far from the test section as possible, with the longest undisturbed approaching air line length achievable. Thus it was placed in the upper third of the exhaust shaft, taking into account noise emissions to the surroundings of the building, as further discussed in subsection 4.

In order to keep pressure losses and therefore power requirements low, another aerodynamic objective of a wind tunnel is to decelerate the flow within the air line as effective as possible. This demands a wide cross section, hence tight integration of the duct into the installation and exhaust shafts. Therefore, accessibility of the downstream wind tunnel legs is very difficult to establish, yet very important for maintenance, cleaning or revision works. [3] The size of the cross section achievable would not allow for walk-through turning vanes, whether they were designed as baffle silencer or not. For this reason, the grids of guiding vanes in the corners one, two and three are mounted in a frame that is hinged and can be pivoted toward the sidewall in order to allow passage of equipment and staff. The cord length of the vanes is therefore limited as is the effectivity of an acoustical treatment of their surfaces. Furthermore corner two is designed as an expanding corner, which is described in section 5. This is due to the given structure enforcing a narrow inlet to this corner, while the downstream exhaust shaft allows for a wider cross section with only short length for a separate diffuser in between.

As a cost-efficient design, a rectangular cross section was chosen for the entire duct, except for the circular drive section and its transitions. The duct itself consists of three functional layers, as shown in figure 4. The outer hull that seals the wind tunnel off the ambient atmosphere, enabling the suction of air through the test section by the drive in the first place. For easier integration into the existing structures, for which sometimes spontaneous and quick adaption is required, it was decided to build this hull from sealed birch plywood. The intermediate layer consists of high-density rock wool for good acoustical absorption over a wide frequency spectrum. The durable inner layer accomplishes the guidance of the flow, defining the duct cross section. It is made from galvanized perforated sheet metal of varying thickness, according to the specific requirements of the given section. The sheets are mounted with construction wood along the outer edges so their secondary function as absorbing resonator is ensured. For integrity of the rock wool, the backside of the perforated panels is lined with a $60\,\mathrm{g/m^2}$ mat of glass fibers that is acoustically transparent.

The aim was to keep the thickness of the absorbing layer as large as possible, in order to ensure sufficient low frequency dampening. The resulting air reservoirs, dampened by the flow resistivity of the absorber, are expected to reduce possible long-wave fluctua-

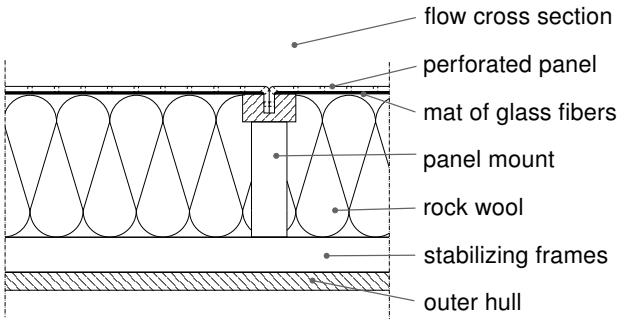

FIG 4. Functional layers of the wind tunnel duct.

tions in flow speed as well. As can be seen from section 4, a major issue might be the dampening of high frequencies due to the bypassing effect above a critical frequency.

3. WIND TUNNEL DIMENSIONING

With the geometric conditions, possible design range and generic design concept known, the sizing of the wind tunnel components is to be accomplished.

3.1. Test Section

As stated before, the largest test section size possible is to be achieved. In this case, it is directly limited by the size of the plenum and implicitly by the size and length of the desired contraction and settling chamber, which need to fit in front of the anechoic chamber. The direct limitation resulting from secondary flows within the plenum alongside with deformation of the free jet by the Coandă-effect were investigated by Deutenbach [4]. The general recommendation to not exceed a nozzle outlet area of a quarter of the plenum cross section needs to be translated from a 3/4-open-jet to this all around open jet, whereas the relative plenum lengths are comparable. The requirement yields minimum distances between the plenum walls and the nozzle exit of 0.3 relative to the plenum edges. This results in a (rounded) maximum nozzle exit height for this tunnel of $0.8\,\mathrm{m}$. As mentioned in section 2.3, the horizontal displacement of the free jet leads to further restrictions in size. Taking this into account the nozzle exit width was determined to be $1.0\,\mathrm{m}$.
In order to meet typical cord Reynolds number of the test objects of interest, as mentioned in section 2.1, a design Reynolds number of $1\,\mathrm{Mio.}$ was specified. Depending on atmospheric conditions, this yields a jet velocity of around $50\,\mathrm{m/s}$, an ultimate design velocity $55\,\mathrm{m/s}$, hence a volume flux of $44\,\mathrm{m^3/s}$.
The length of the test section is determined by growth and entrainment of the open jet shear layer into the jet core. Taking into account a typical angle of $4°$ to the flow axis [5], the area of the potential flow core is reduced to an area of $35\,\%$ of the nozzle exit area after traveling $2.6\,\mathrm{m}$. This is considerably small for undertaking any reliable flow measurements in the wake of a test object. Taking into account an installation depth for the collector plus a certain space for probe mounting, the contraction was shifted further downstream into plenum, cf. figure 3, in order to achieve mentioned jet length and gain additional space for a smooth intake in front of the honeycomb flow straightener.

3.2. Contraction, Settling Chamber, Inlet

A decisive factor for the quality of the flow within the test section is the contraction, which by great contraction ratios reduces the relative magnitude of turbulence compared to the main flow. A secondary positive effect is a low flow velocity in the settling chamber, yielding lower pressure loss over honeycomb and screens as well as reducing their noise emissions. The latter are increasing with the flow velocity by the power of 6 [6]. Therefore, the contraction ratio was increased up to the limit of the installation space and a value of 8 : 1 was established.
Due to limited space, the shortest nozzle shape possible without flow separation is of special interest. The design by Börger [7] was considered at first, however ultimately neglected since it is only directly applicable to circular ducts and of critical robustness against disturbing factors, being designed at the very threshold of the possible. Therefore, a more resilient design with a total length of $2.85\,\mathrm{m}$ was chosen.
Within the $1.48\,\mathrm{m}$ long settling chamber a honeycomb flow straightener made from phenolic resin-impregnated paper is planed. With a cell width of $6.4\,\mathrm{mm}$ and a length of $110\,\mathrm{mm}$, an excellent length-to-diameter ratio of 17 is reached.
Downstream of the honeycomb, two turbulence screens will be placed. For dimensioning, the product ranges of several suppliers were reviewed and the pressure loss coefficients were determined [8], the recommended value being 1 [3]. From an acoustical point of view it is to be mentioned that noise emissions are increasing with the pressure loss coefficient by the power of 3 [6]. A good example to start with is a $0.63\,\mathrm{mm}$ gauge wire screen with a mesh aperture of $2.0\,\mathrm{mm}$. Several products come in to question so that in the end it can be decided according to the price.
For the inlet lips, the conclusions of Johl [9] were used to design an elliptic bell mouth with an axis ratio of 2 for good flow attachment.

3.3. Collector

The detailed specific collector sizing is jet to be finalized since it is a complex and crucial element for open-jet wind tunnels [10]. Therefore, it will be subject to further investigation. However, it is planned to incorporate lifting-wing-profiled surfaces, adjustable in pitch and distance in order to establish optimal settings in respective to the jet's pressure profile and noise.

3.4. Corners

As mentioned in section 2.3, the corner vanes are to be designed with short cord length due to available space. For a cost-efficient design, guide vanes made of simple sheet metal arches are the durable go-to solution. However, the first corner is in line of sight to the test section and prone to unsteady inflow due to the wake of test objects. For a more robust behavior compared to sheet metal arches with relatively sharp leading edges, profiled guide vanes of simple geometry were selected [11]. These can be manufactured using only three different radii. The cascade consists of 15 vanes with a cord of 220 mm which are extended with a trailing edge tab to eliminate a direct line-of-sight through the cascade for acoustical reasons.
Corners two and three will encounter less critical inflow and are therefore designed as circular-arc vanes [3], following a design by Bradshaw and Pankhurst [12] with a gap-cord ratio of 0.35. The more detailed layout of corner two toward an expanding corner is described in section 5.
The wake-uniformity of the outlet bend downstream of the drive is uncritical for the overall flow quality and noise level of the wind tunnel. In order to reduce construction effort in this hard-to-reach area, a design of a short radius elbow with two vanes was selected [13], even more so since the existing lining structure of the exhaust duct favored this solution as well.

3.5. Power Requirement

The diffusers were designed in a way that they would not exceed an equivalent cone angle of 3° [3] in order to ensure robustness against flow separation. The given building space limited the area ratios of the diffuser legs in such a way that the dimensions of the final exhaust duct only could be reached after a succession of one dimensional expansions, enabling a cost-efficient construction work jet again.
With the geometries of the air duct known, the pressure loss of each wind tunnel component was calculated by the use of handbook methods [3]. The resulting progression of static pressure, total pressure and mean velocity is shown in figure 5. These values yield information on pressure loads on the hull of each segment, holding forces for components like corner vanes and, most importantly, the design point for the wind tunnel drive. It has to deliver the required volume flux of 44 m^3/s over a pressure rise of about 1 500 Pa, resulting in a power requirement of 70 kW. The power factor of the wind tunnel therefore is approximately 0.88.
Because of the relatively high pressure leap required, a radial compressor was considered due to the lower noise emissions of such a design compared to an axial fan. Additionally, the inclusive flow deflection by 90° could substitute a corner. However, it had to be dismissed because of insufficient building space for a radial machine that could deliver the required volume flux. Therefore, an axial fan for vertical installation was chosen for this wind tunnel.

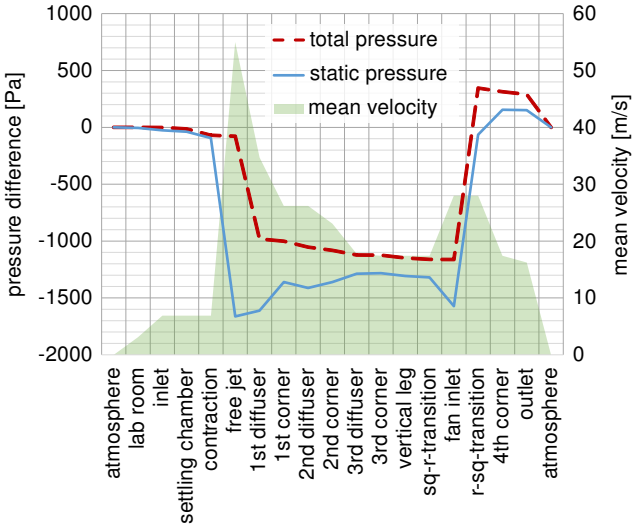

FIG 5. Profile of static pressure, total pressure and mean velocity throughout the air line of the wind tunnel

Budget limitations favor a production model out of the 'heating, ventilation, and air conditioning' segment with variable speed control rather than a custom-made fan for this project. Building space allowed for a maximum nominal fan diameter of 1.4 m, which was chosen, as well as a construction with stator vanes. The benefits of which are a more efficient flow through the exit elbow, a greater pressure rise at lower engine speed and better reserves toward higher pressure ratios. Taking into account efficiency factors of 0.77 for the fan and 0.95 for the electric engine, its required electric power is around 96 kW. In order to provide power reserves, a 110 kW-engine was chosen, since the building size of which stayed constant, giving some security without significant rise in costs.
To ensure a low pressure loss downstream of the engine itself, a central cone of 2 m length is mounted on top of the electric engine, constituting a ring diffuser [14] together with the outer transition from a round to square cross section. The cone as well is acoustically treated in order to reduce noise emissions to the outside and enable an installation of the fan further downstream. The acoustical considerations for this positioning are described in the following section.

4. FAN POSITIONING

The Sixth General Administrative Regulation on the Federal Immission Control Act constitutes a maximum noise immission of 60 dB(A) within the relevant area and time of day for the facility [15]. As there is a residential building 35 m opposite and about 30° below the outlet, it is an important step, within the preliminary design phase, to ensure compliance of the dampening concept with the applicable limit values.
Calculation of the immission values spreads over four sections: the absorption path within the ring diffuser and remaining square duct, the dampening through

the 90°-elbow, additional noise generation by the free jet and finally the sound propagation to the next possible receiver. The resulting evolution of the emission spectrum is depicted in figure 6.
In a first step, spectra for the absorption coefficient α of the lined surfaces are determined using a freely available, reviewed calculation tool [16]. However in a ducted flow, these surfaces do not absorb sound completely according to their spectra since noise above a critical cut-off frequency f_c radiates through the duct without losing significant amounts of energy to the outer surfaces:

$$f_c = \frac{2c}{b}. \tag{1}$$

This value depends on the speed of sound c and the gap between to opposite absorbing surfaces b. By utilization of the Piening's formula, the dampening value D of each section Δx is calculated per octave frequency f [6] [17]:

$$D_{\Delta x} = 1.5 \cdot \frac{O}{S} \cdot \alpha\,(f) \cdot \Delta x \cdot \begin{cases} \left(\frac{f_c}{f}\right)^2 & \text{dB} \quad \forall f > f_c \\ 1 & \text{dB} \quad \forall f \leq f_c \end{cases} \tag{2}$$

with the circumference of lining O and the free cross section area S. The results are subtracted from the respective upstream emission spectrum, beginning with the noise emission spectrum of the fan provided by the manufacturer.

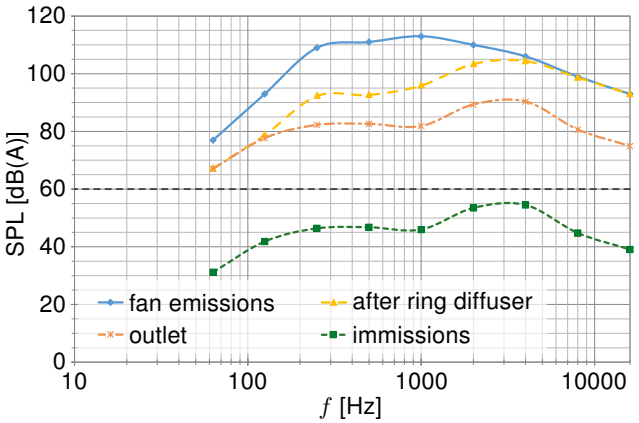

FIG 6. Successive dampening of sound pressure levels over the frequency spectrum

For the outlet elbow, another critical frequency applies in correspondence to the gap b between the guide vanes. As a conservative estimation of the sound pressure alteration over the elbow, dampening values were taken from VDI 2081 [18] for a duct with lining and guide vanes.
The free jet sound pressure level (SPL) originating from the turbulent shear layer of the outlet flow $L_{W,jet}$ was calculated with the method presented in [10] for low Mach numbers M:

$$L_{W,jet} = 142.7 + 10\log\left(\frac{S}{\mathrm{m}^2}\right) + 60\log\,(M) \quad \text{dB}. \tag{3}$$

Using a reference spectrum, this is distributed over the octaves, A-filtered and logarithmically added to the already established SPL. With $53\,\mathrm{dB(A)}$, the jet noise is relatively low compared to the SPL of the fan radiating from the outlet and does not lead to a critical increase in noise.
In the last step, the noise immission for the receiver L_i was calculated taking into account the dispersion of acoustic energy as a quarter of a sphere with radius r as well as the directivity DI across the frequency spectrum for the given circumstances [17]:

$$L_i = L_{W,out} - 20\log\,(r) - 5 + DI(f) \quad \text{dB}. \tag{4}$$

The boundary conditions are quite conservative since partial shading of the direct path is done by the building's roof as well as there is no continuous wall in the plane of the outlet enclosing the quarter of the sphere. As can be derived from the intermediate results of figure 6, frequencies between $2\,\mathrm{kHz}$ and $4\,\mathrm{kHz}$ are critical for the overall immission sound pressure level. With the developed calculation method, it could be shown that mounting the fan further upstream would not dampen these frequencies since they are directly radiating through the present duct. Additional $30\,\mathrm{mm}$-thick lining of the inner surfaces of the elbow vanes, however, would systematically suppress outward reflection of the critical noise. [17] Therefore, this supplementary treatment is preferred to bringing the fan closer to the third corner of the wind tunnel, which would lead to a more disturbed inflow, hence even more noise. With the plane of the fan being ultimately fixed $5.5\,\mathrm{m}$ below the outlet, an immission SPL of $59\,\mathrm{dB(A)}$ could be calculated with conservative assumptions, which would qualify the facility for continuous operation during daytime hours.

5. EXPANDING CORNER

Another detailed investigation was carried out on the second corner of this wind tunnel. The given structure of the building enforces a narrow inlet to this corner, while the downstream exhaust shaft allows for a wider cross section. With only a short duct length between the second and third corner, an additional diffuser would be necessary in order to reach the planned exhaust shaft dimensions. With an expanding second corner, a straight, easier-to-build wall structure could be enabled downstream of corner three, which moreover would encounter lower velocities, hence lower pressure losses. The necessary expansion ratio of $e = 1.32$ is an achievable aim, however the flow can be prone to detachment due to the deceleration [19]. Therefore, an iterative alteration of the baseline design of the second corner towards an expanding configuration was performed by the utilization of CFD methods. The overall objective was to obtain a uniform velocity distribution at the center plane of the following corner as well as a simple design with many identical parts for cost effectiveness.

5.1. CFD Method

For this investigation it was aimed for an accurate two-dimensional simulation of the flow through the corner vane cascade, using the DLR TAU code [20]. The code is an unstructured finite volume solver for the compressible Reynolds-Averaged Navier-Stokes (RANS) equations and contains a variety of RANS turbulence models, of which the Menter SST two-equation model (SST-2003) was applied. The CENTAUR [21] mesh generator is used for the spatial discretization of the simulation by means a hybrid mesh. While quad layers resolve the boundary layers of the outer walls and the vanes, the free stream is discretized with triangles which are refined in critical areas of the flow, especially around the outer vanes.
In order to obtain realistic inflow conditions, especially in terms of boundary layers, the entire length of the upstream diffuser was modeled as well. For a mitigation of interference effects with the outlet surface, the downstream leg was elongated, giving the opportunity to evaluate the development of the flow uniformity. To ensure the accuracy of the simulation, several mesh studies were executed beforehand as well as a comparison with a high-resolution three-dimensional simulation of periodic vane cascade, for a comparison of the detachment behavior. After receiving satisfactory results, the studies continued with two-dimensional simulations. Besides the alterations of the geometry, the inflow velocity was varied as well to ensure good performance of the design throughout the wind tunnel's envelope. In the following, the results for the highest velocities with a Reynolds number 425 000 for the vane's arc length of 240 mm are presented.

5.2. Results

First of all, the baseline design of the corner with no expansion was simulated and analyzed. As can be seen in the contour plot of the absolute flow velocity normalized by the approach velocity u_∞ in figure 7, the volume flux through the cascade is higher on the inside. This is due to the thickening of the boundary layer in the outer corner while the flow is dammed up by the concave deflection up to a point where a small recirculation zone is formed. Downstream of the vanes, the imbalanced flux is evened out after a distance of half the duct width. Streamlines indicate a rather clean 90° bend of the flow on the entire length of the cascade. Despite some negligible ares of leading edge flow separation due to sharp edges, the airflow around the corner vanes is attached. Furthermore, it can be seen that the angle of attack decreases from the inside out.
The expansion ratio of the corner was increased by widening the outlet area and distributing the vanes on the diagonal with the same orientation as the baseline, creating an expanding channel between every vane. The results in figure 8 show a stronger retardation of the flow through the outer bend and a significantly larger area of recirculation. Due to this, the volume flux on the suction side of the outermost

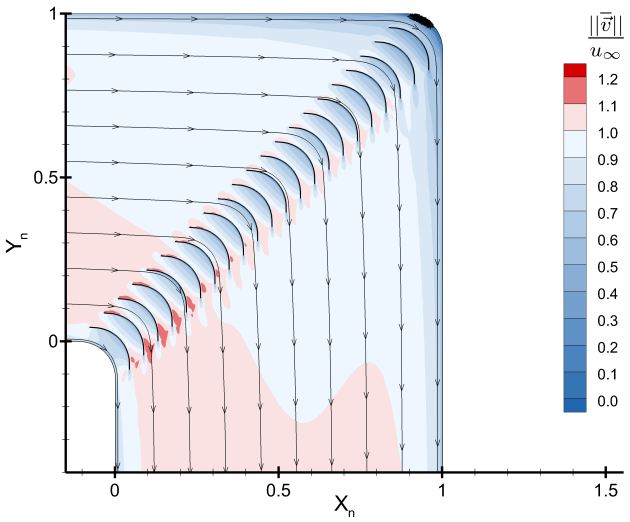

FIG 7. Contour plot of the simulated flow through the baseline design of the second corner. Geometry normalized by inlet width.

vane is very low. This corresponds to the streamlines that indicate a flux deficit on the outer side since they are bend by less than 90°, filling up this deficit downstream of the vane cascade.

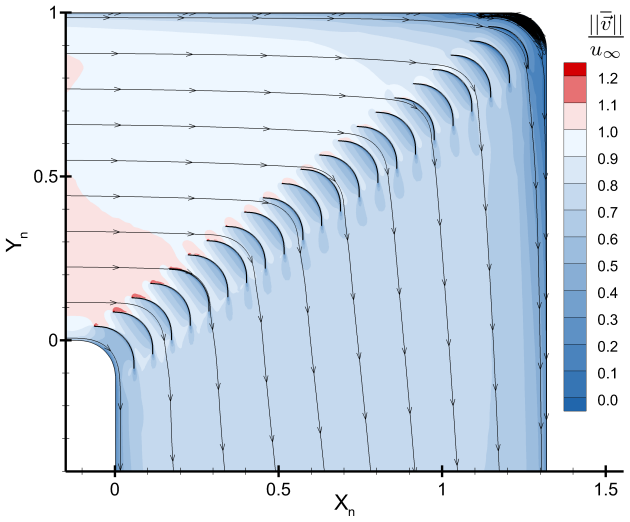

FIG 8. Contour plot of the simulated flow through the expanding corner baseline. Geometry normalized by inlet width.

In order to reduce this imbalance in volume flux, an attempt was made, to deduce a design that would suppress the occurrence of any separation area along the outer edge of the corner. It was found that the increase of the outer wall's radius would lead to this result, which on the other hand requires the removal of vanes. At the same time, the inflow is deflected more significantly by the outside surface before entering the vane cascade. Consequently, several of the outer vanes were shortened to retain a positive angle of attack. The tendency of the streamlines toward the outside wall, however, could not be omitted completely. The expansion ratio of the cascade was therefore reduced and substituted by sloping the outer

downstream wall up to the final width of the cross section. This supported the mitigation of flow detachment as well.
The resulting design and the corresponding flow simulation is depicted in figure 9, where no recirculation zone occurs. Instead, the boundary layer of the outside wall gets accelerated and flattened out rather quickly. The tendency of the flow against this surface additionally stabilizes the otherwise critical boundary layers of diffusers. Considering the inflow, a more uniform distribution of volume flux can be observed, combined with more similar angle of attacks. The outer vane of baseline design encounters higher velocities; however has an uncritical angle of attack. In respect to the design goal of a simple design, the use of only two different vane shapes shall be preserved at this point.

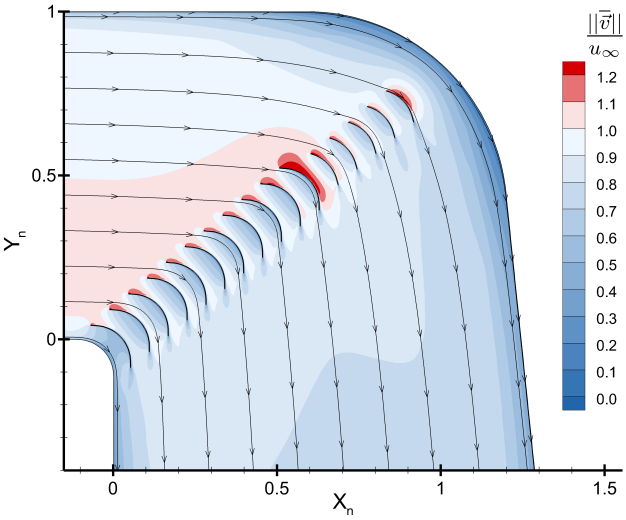

FIG 9. Contour plot of the simulated flow through the expanding corner variant with a wide outer contour, migrating into an asymmetrical diffuser. Geometry normalized by inlet width.

For better comparison of the performance of the several corner designs, the absolute flow velocities in main direction were determined along the center line of the following corner ($Y_n = -1.5$), normalized by the inflow velocity and scaled with the expansion ratio e in order to enable a comparison with the baseline. The results, plotted over the relative width of the outlet, are depicted in figure 10. For the baseline expanding corner, the over- respectively the undershoot of about 5 % can be seen along the duct width. The alternative design with the widened outer radius yields a more uniform profile, similar to the original baseline. However, the differences are rather small so that either design of the expanding corner is unlikely to lead to a critical inflow to the fan. Nevertheless, the alternative design enables the reduction of vanes as well as an increase in projected absorption surface for noise traveling upstream. Therefore it was decided to incorporate this design for this wind tunnel.
Since the recirculation zone at the outer radius is very likely a general issue with these kinds of lined corners, this newly design can be an interesting proposal

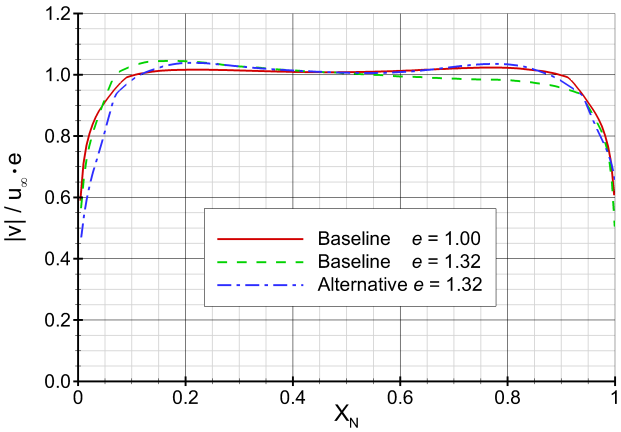

FIG 10. Comparison of velocity profiles at the centerline of corner three. Geometry normalized by outlet width.

for expanding corners that can be equipped with individual turning vanes an easily accessed for confirmatory measurements. This way, corresponding with a subsequent diffuser, an absolute optimum might be found in order to expand with the highest ratio possible. Especially closed-loop wind tunnels profit from an efficient usage of building space.

6. CONCLUSION AND OUTLOOK

The design concept of the new aeroacoustic wind tunnel of the ILR at RWTH Aachen University was presented. It is an open-circuit, open-jet type facility with a high contraction ratio that will complement the existing testing infrastructure of the institute by a further wind tunnel with excellent flow quality and low-noise properties. With the application of several state-of-the-art measurement technologies, such as microphone arrays and time resolved quantitative flow measurement, the facility will make a lasting contribution to expanding the knowledge of aeroacoustic phenomena, both on the academic experimental model and on the concrete product.
Integration of the wind tunnel into the existing structure was successfully executed, sizing a wind tunnel with optimum utilization of available space. The positioning of the fan, due to acoustical considerations, as well as the design of an expanding corner, due to geometrical conditions, were demonstrated.
Further investigation will be conducted on the detailed collector design toward an optimal design considering flow quality and noise. Moreover, specific optimization will be carried out, once the facility goes into operation.

Contact address:

sebastian.hille@ilr.rwth-achen.de

References

[1] P. B. S. Lissaman. Low-reynolds-number airfoils. *Annual Review of Fluid Mechanics*, 15:223–239, 1983. DOI: 10.1146/annurev.fl.15.010183.001255.

[2] G+H Schallschutz GmbH. Sonex wf flachabsorber: für hochabsorbierende räume iso 3744 und für reflexionsarme räume iso 3745 mit breitbandigen schallquellen, 2017.

[3] Jewel B. Barlow, William H. Rae, and Alan Pope. *Low-speed wind tunnel testing*. Wiley, New York, NY, 3. ed. edition, 1999. ISBN: 0471557749.

[4] K.-R. Deutenbach. Influence of plenum dimensions on drag measurements in 3/4-open-jet automotive wind tunnels. *SAE Transactions, Section 6: Journal of Passenger Cars*, (104):1800–1809, 1995.

[5] Vlad Ciobaca, Michael Pott Pollenske, Stefan Melber Wilkending, and Georg Wichmann. Computational and experimental results in the open test section of the aeroacoustic windtunnel braunschweig. *International Journal of Engineering Systems Modelling and Simulation*, 5(1/2/3):125, 2013. DOI: 10.1504/IJESMS.2013.052385.

[6] Manfred Heckl, editor. *Taschenbuch der technischen Akustik*. Springer, Berlin, 2. aufl., korrigierter nachdr edition, 1995. ISBN: 9783642973574. DOI: 10.1007/978-3-642-97356-7.

[7] G.-G. Börger. Optimierung von windkanaldüsen für den ungterschallbereich. *Zeitschrift für Flugwissenschaften*, 23(2):45–50, 1975.

[8] W. Bohl and W. Elmendorf. *Technische Strömungslehre: Stoffeigenschaften von Flüssigkeiten und Gasen, Hydrostatik, Aerostatik, Inkompressible Strömungen, Kompressible Strömungen, Strömungsmesstechnik: Fachbuch Kamprath-Reihe*. Vogel, Würzburg, 13 edition, 2005. ISBN: 978-3-8343-3029-1.

[9] G. Johl. *The design and performance of a 1.9m x 1.3m indraft wind tunnel*. Doctoral thesis, Loughborough University, Loughborough, 2010.

[10] Jochen Wiedemann, Gerhard Wickern, Bernd Ewald, and Christof Mattern. Audi aero-acoustic wind tunnel. In *SAE Technical Paper Series*, SAE Technical Paper Series. SAE International400 Commonwealth Drive, Warrendale, PA, United States, 1993. DOI: 10.4271/930300.

[11] T. F. Gelder, R. D. Moore, J. M. Sanz, and E. R. Mcfarland. Wind tunnel turning vanes of modern design. *AIAA: Aerospace Sciences Meeting*, 24, 1986.

[12] P. Bradshaw and R. C. Pankhurst. The design of low-speed wind tunnels. *Progress in Aerospace Sciences*, 5:1–69, 1964. DOI: 10.1016/0376-0421(64)90003-X.

[13] Department of Veterans Affairs. Ductwork radius elbows, 2008.

[14] W. Bohl. *Strömungsmaschinen: Berechnung und Konstruktion*. Vogel-Fachbuch. Vogel, Würzburg, 1980.

[15] Bundesministerium für Umwelt, Naturschutz und Reaktorsicherheit. Sechste allgemeine verwaltungsvorschrift zum bundesimmissionsschutzgesetz: Technische anleitung zum schutz gegen lärm - ta lärm, 2017.

[16] C. Whealy. Porous absorber calculator v1.59, 2012.

[17] Helmut V. Fuchs. *Schallabsorber und Schalldämpfer: Innovative akustische Konzepte und Bauteile mit praktischen Anwendungen in konkreten Beispielen*. VDI-Buch. Springer, Berlin, 3., wesentlich erweiterte und aktualisierte aufl. edition, 2010. ISBN: 978-3-642-01412-3. DOI: 10.1007/978-3-642-01413-0.

[18] Verein Deutscher Ingenieure. Raumlufttechnik: Geräuscherzeugung und lärmminderung, 2019.

[19] Björn Lindgren and Arne V. Johansson. Design and evaluation of a low-speed wind tunnel with expanding corners.

[20] D. Schwamborn, T. Gerhold, and R. Heinrich. The dlr tau-code: Recent applications in research and industry. In *ECCOMAS CFD 2006 CONFERENCE*, 2006.

[21] CentaurSoft. Centaur software: Mesh (grid) generation for cfd and computational simulations, 20.08.2020.